



A combined cathodoluminescence and electron backscatter diffraction examination of the growth relationships between Jwaneng diamonds and their eclogitic inclusions

Gareth R. Davies¹ · Quint van den Heuvel¹ · Sergei Matveev² · Martyn R. Drury² · Ingrid L. Chinn³ · Michael U. Gress¹

Received: 23 November 2017 / Accepted: 28 August 2018 / Published online: 18 September 2018
© The Author(s) 2018

Abstract

To fully understand the implications of the compositional information recorded by inclusions in diamond it is vital to know if their growth was syn- or protogenetic and the extent to which they have equilibrated with diamond forming agents. The current paradigm is that the majority of inclusions in diamond are syngenetic but recently this assumption has been questioned. This study presents an integrated cathodoluminescence (CL) and electron backscatter diffraction (EBSD) study of 8 diamonds containing eclogitic inclusions: 19 pyrope-almandine garnets, 12 omphacitic clinopyroxenes, 4 sulphides, 1 coesite and 1 rutile from the Jwaneng diamond mine, Botswana. Diamond plates were sequentially polished to expose inclusions at different levels and CL imaging and EBSD were performed to constrain the relationship between diamond and inclusion growth. Despite complex growth and resorption, individual diamonds are single crystals with a homogeneous crystallographic orientation. All individual inclusions have homogeneous crystallographic orientation and no resolvable compositional zonation. The combined CL and EBSD data suggest that epitaxial inclusion-diamond growth is rare (none of 24 inclusions) and that the imposition of cubo-octahedral faces on inclusions does not necessarily result in epitaxy. Individual diamonds contain inclusions that record evidence of both syngenetic and protogenetic relationships with the host diamond and in one case an inclusion appears syngenetic to the diamond core but protogenetic to the growth zone that surrounds 70% of the inclusion. These findings emphasise that inclusions in diamonds have multiple modes of origin and that in order to validate the significance of geochronological studies, further work is needed to establish that there is rapid chemical equilibration of protogenetic inclusions with diamond forming agents at mantle temperatures.

Keywords Diamond · Silicate inclusion · Syngenetic · Protogenetic

Introduction

Mineral inclusions in diamond are potentially fundamental to understanding the formation conditions of diamond and Earth's

long-term volatile cycles (Shirey et al. 2013). However, in order to fully understand the implications of the compositional information recorded by inclusions it is vital to know the processes that caused inclusion growth and the extent to which they have equilibrated with the diamond forming agent; i.e., if they are proto-, syn-, or epi-genetic. In the latter context Nestola et al. (2017) have recently proposed the use of the term synchronous for the situation where a protogenetic phase records the time of diamond growth by achieving equilibration with the diamond-forming agent. The current paradigm, however, is that the majority of diamond inclusions are syngenetic, based on the cubo-octahedral morphology imposed on the inclusions (e.g., Harris and Gurney 1979) and crystallographic controlled relationships (epitaxy) between host diamond and inclusions (e.g., Harris and Gurney 1979; Wiggers de Vries et al. 2011). Recent work, however, has questioned this assumption and reported that the crystallographic relationships between inclusions and the host diamond are highly complex (Agrosi et al. 2016). The lack of crystallographic control

Editorial handling: T. Stachel

Electronic supplementary material The online version of this article (<https://doi.org/10.1007/s00710-018-0634-3>) contains supplementary material, which is available to authorized users.

✉ Gareth R. Davies
g.r.davies@vu.nl

¹ Vrije Universiteit, De Boelelaan 1085, 1081, HV Amsterdam, The Netherlands

² Faculty of Geosciences, Utrecht University, 3584, CB Utrecht, The Netherlands

³ De Beers Exploration, Private Bag X01, Southdale, Johannesburg 2135, South Africa

between olivine inclusions and host diamond has been used to question the significance of imposed diamond morphology (Nestola et al. 2014). Additionally the same group (Bruno et al. 2016) reported that there is no thermodynamic benefit for olivine and diamond to form epitaxially as there is no difference in adhesion energies between diamond and forsterite. Hence, even during synchronous growth there is no reason to develop preferential orientations. This conclusion appears to contrast with reports of preferred orientation and epitaxial growth of olivine inclusions in diamond by Neuser et al. (2015). Milani et al. (2016), however, re-interpreted these data and concluded that there was no epitaxy between olivine and the host diamonds.

To provide further constraints on the growth relationship of silicate inclusions and host diamond, this study presents integrated cathodoluminescence (CL) and electron backscatter diffraction (EBSD) data of eight inclusion-bearing diamonds. Diamond growth zonation is studied using CL imaging performed at different depths in order to constrain three-dimensional diamond growth around the inclusions and analyse the crystallographic orientation of the host diamond and inclusions by EBSD. The aim is to better assess what information determined from an inclusion (e.g., P-T, geochemical environment, age) can also be applied to the diamond host and how well inclusion populations must be characterised in order to perform geochronological studies.

Samples and analyses

Sample selection

In a companion paper, Gress et al. (2018) present an extensive study of run of mine production from the Jwaneng diamond mine, Botswana. That study reports representative diamond growth histories based on CL images and infrared spectroscopy and silicate inclusion compositions. In our study, eight additional multiple silicate inclusion-bearing diamonds were selected from Jwaneng. The eight diamonds contain 37 eclogitic inclusions: 19 pyrope-almandine garnets, 12 omphacitic clinopyroxenes, 4 sulphides, 1 coesite and 1 rutile. Twenty-four silicate and oxide inclusions were exposed by sequential polishing and varied from 8 μm to $\sim 150 \mu\text{m}$ in size. They generally occurred as isolated inclusions distributed in central to intermediate growth zones of the diamonds.

Analytical methods

Cathodoluminescence (CL)

Diamond plates were produced by laser cutting through the centre of eight individual diamonds. In order to include multiple inclusions not all plates were cut exactly along the $\{110\}$ crystal

lattice plane (deviation up to 15°). Cathodoluminescence imaging was performed on a JEOL JXA-8530F field emission electron probe microanalyser (FE-EPMA) fitted with a panchromatic JEOL CL. Imaging was undertaken with an acceleration voltage of 10 kV and a beam current of 5 pA. Additional high resolution CL imaging of the growth zones directly around inclusions was performed with a Gatan retractable panchromatic CL attached to the Helios Nanolab G3 UC system capable of $<250 \text{ nm}$ spot size at 5 kV with a beam current of 0.8 nA.

Composite CL images were made of each diamond plate and detailed CL images taken around individual inclusions following different polishing stages. The terminology followed is to define the core as the oldest part of the diamond and subdivide core, intermediate and rim regions if there are well-defined interfaces; individual inclusions from the same diamond are numbered alphabetically. Samples JW288 and JW334 were only polished once.

Electron backscatter diffraction

Standard diamond polishing techniques damaged inclusions to such a degree that electron backscatter diffraction (EBSD) measurements were impossible. The inclusions were therefore milled with a Ga + focused ion beam (FIB) at a 12° angle to clean surfaces. The EBSD technique allows measurement of the orientation of single crystal grains as small as 1 μm with a 1° uncertainty (Prior et al. 1999). A Helios Nanolab G3 UC instrument produces an omni-directional source of scattered electrons. Diffraction of these electrons occur simultaneously on all the lattice planes of the sample. The backscattered electrons (BSE) that escape the sample form a diffraction pattern of Kikuchi lines that is visualized on a phosphorous screen fitted to the EBSD detector. This makes EBSD a powerful tool for in situ crystallographic measurements of inclusions on a micron scale. An example of an EBSD pattern is presented in Fig. S1 showing Kikuchi lines for rutile with some intersections labelled. In addition, Fig. S1 includes an example of raw EBSD data projected on a lower hemisphere stereographic projection of the three principal crystal lattice planes of diamond.

EBSD data are plotted in the spatial co-ordinate system with orthogonal reference axes, X, Y and Z, defined by the microscope stage. The orientation of the major crystallographic axes for diamond and inclusions are presented in stereographic projections showing the X and Y axes. Each crystal orientation will plot as a number of poles, depending on the crystal structure of the phase. For the cubic phases diamond and garnet, one crystal orientation has three $[100]$ axes, six $[110]$ axes, and four $[111]$ axes. If there was an epitaxial relationship between host and inclusion then the crystal axes of host and inclusion would all be parallel. An additional method to compare the orientation of 2 phases is to use their Euler angles. The Euler angles describe the orientation of a rigid body with respect to a fixed coordinate system (see Bunge

1993). If the Euler angles are equivalent, or related by the symmetry of one of the phases, then the phases are epitaxial.

High resolution transmission electron microscope (TEM) imaging was performed on an inclusion-diamond contact with a Talos F200X operating at 200 kV. Scanning TEM analysis was used to determine if volumes of the diamond close to the diamond-inclusion contact contained elemental impurities.

Electron probe microanalysis

Exposed inclusions were subjected EPMA on a JEOL JXA-8350F instrument. The diamond plates were placed on double sided carbon sticky-tape and a carbon coating was applied to prevent charging. Measurements were performed with an acceleration voltage of 15 kV, beam current of 25 nA and focal spot diameter set to 1 μm . Further details of instrument set up can be found in Timmerman et al. (2015, 2018 and references therein). Raw data were processed using Probe for EPMA software package. The PAP full (Original) Phi(rho-Z) correction was applied using the FFAST table of Mass Absorption Coefficients (Chantler et al 2005). Detection limits were better than 300 wt.ppm (99% confidence level). Accuracy was checked by measuring primary standards before and after a series of 50 points on unknown samples and was better than $\pm 1\%$ relative. More details on data treatment is given elsewhere (Timmerman et al. 2015 and references therein). In spite of FIB milling, inclusion surfaces were not adequate for high-precision EMPA measurements and therefore the inclusions were treated as unpolished minerals and data evaluated following a protocol described in Timmerman et al. (2015). Compositions of the mineral inclusions are reported in Tables S1 and S2.

Results

Visual observation showed that of the 24 analysed inclusions 14 have some planar crystal faces and of these 6 have partial development of cubo-octahedral morphology (JW078B and C; JW204B and D and JW356D and F) that could have been

imposed by the diamond. None of the inclusions records full cubo-octahedral morphology.

Detailed descriptions of inclusion-diamond relationships are reported below and summarised in Table 1. JW012 is a garnet- and omphacite-bearing diamond with octahedral growth around the two garnet inclusions and a later rim of diamond with dull luminescence, separated by a resorption event (to the left in Fig. 1a). The centre and intermediate regions of the plate contain irregular areas ($\sim 25\%$) with lower nitrogen (grey in black and white images <150 at.ppm N), while the outer regions consistently show higher nitrogen contents. Both inclusions occur near the centre of the plate with B having an ovoid subhedral shape with maximum dimensions of $\sim 70 \times 90$ μm (Fig. 1b) with interrupted nested octahedral diamond growth layers surrounding the inclusion. The generally ovoid subhedral inclusion C has a triangular termination at one end with two well defined crystal faces (maximum dimensions of $\sim 50 \times 80$ μm Fig. 1c). Within ~ 10 to 20 μm of the inclusions, diamond growth layers are poorly defined with a mottled/diffuse appearance, named CL halo (Figs. 1b, c). At a larger scale (> 20 μm), extension of well-defined planar octahedral diamond growth layers through the CL halo would intersect the garnet inclusion. Similar diamond growth relationships are defined by garnet C with the notable observation that there are triangular growth layers that are parallel to the triangular termination of the inclusion. There is no coincidence in crystallographic orientation between the inclusions and the host diamond (Figs. 2a,b).

Garnet- and omphacite-bearing dodecahedron JW078 has no clear CL growth pattern except for octahedral growth, most obviously in the rim at the bottom and upper left edge of the plate (Fig. S2a). Both exposed subhedral garnets have some well-developed crystal faces. Inclusion B has an overall cubic shape whereas C has cubo-octahedral faces on the right hand side (Figs. S2b,c). There are no coincidences in major crystal axes between the diamond and inclusion B although the [100] axes for garnet C show an apparent mirror pattern with the diamond [100] (within 1° , Fig. S2e; Table S3).

Table 1 Summary of inclusion growth forms and relationships with host diamond

Sample No.	Good crystal faces	Poor crystal faces	Enclosed by growth	Cutting diamond growth	Influenced diamond growth	Aligned with diamond growth	In poorly defined growth
JW012	B,C	B,C	B,C		C		B,C
JW078	B,C	B, C				C	B,C
JW145	C	C	C				C
JW204	B,C,D,E,G,H	B,D,F1,2,G,H	G	C,D,F1,2,H	D,E	C,E,G,H	B,D,E,F1,2,H
JW288	B					B	
JW334		B	B,C			B	B
JW338	B,C	B	C	B		B,C	C
JW356	B,C,D,E,F,G	B,C,D,E	B,C,D,E,G	E,F,G	E	E,F,G	B,D,F,G

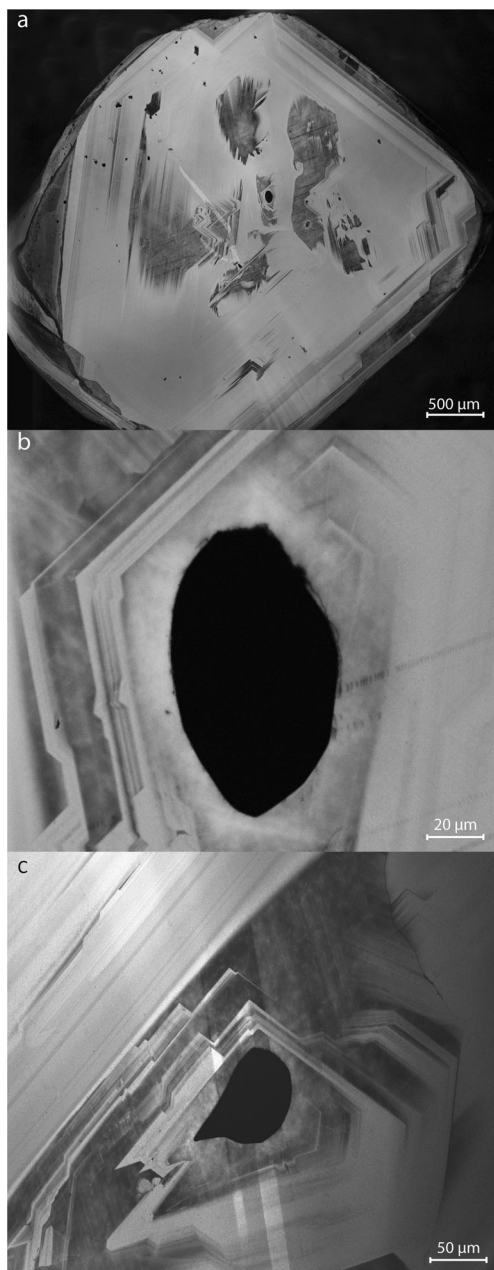


Fig. 1 **a** Composite CL image of a central plate through garnet- and omphacite-bearing diamond octahedron JW012. **b** a close up of inclusion B. **c** a close up of inclusion C exposed by second polish in the area of octahedral growth to the right of inclusion B. The lighter stripes running through image c) are milling artefacts

Octahedron JW145 is garnet-bearing with a complex octahedral central growth structure and regular octahedral growth in the rim (Fig. S3a). The elongated ovoid subhedral garnet was exposed at different levels and reaches 100 µm in size (Figs. S3). There is polishing damage around the inclusion, which appears to have well defined crystal faces on the bottom and left sides (Fig. S3c). The garnet is in dark CL region (low nitrogen; < 150 at.ppm) and surrounded by a bright CL halo and enclosed by octahedral growth layers. At both levels of exposure diamond growth layers adjacent to the inclusion are

discontinuous but generally follow the shape of the inclusion and go around it on the left, whilst growth zones are cut off by the inclusion on the upper right (Fig. S3b: note 90° rotation between Figs. S3b,c). The pole figures show no coincidences between diamond and garnet (one near coincidence, ~5° relative to {112} diamond plane, Figs S3d,e).

Diamond JW204 is octahedral shaped and garnet-, omphacite- and sulphide-bearing (Fig. 3a). The inner core of the sample shows a marked resorption surface before partial and then full octahedral growth. Within this region nitrogen contents generally decreases from core to outer core. The zone around the outer core (intermediate region) has a higher nitrogen content in the octahedral growth layers that gradually decreases towards the edge of the plate. The top right and bottom left apices of the outer growth layers show hummocky cuboid growth. The studied inclusions occur in the core/outer core. Garnet inclusion B (Fig. 3b) has a generally ovoid subhedral shape with a rounded top but four cubo-octahedral faces developed at the base (Fig. 3b). The inclusion occurs in the outer core below the resorbed inner core in a growth zone with no significant growth features. The elongated garnet inclusion C (~70 µm) is situated to the right of the outer core with the long faces parallel to local diamond growth zones but the bottom tip of the mineral cuts a diamond growth zone that is inclined to the majority of the local growth (Fig. 3c). The ovoid subhedral garnet inclusion D cuts the boundary between the inner (on the left) and outer core (Fig. 3d). The ‘base’ of the growth zone is lodged in the inner core of the diamond, associated with two additional grains that are too small to analyse. The base of the grain has three well-developed crystal faces, while the larger part of the inclusion in the outer core has slightly curved crystal faces. Despite a CL halo it is evident that initial diamond growth at the inner core boundary is poorly defined (mottled appearance) but well-developed diamond growth zones to the right of the inclusion are associated with more irregular diamond growth that potentially nucleated from the inclusion surface (Fig. 3d).

Subhedral garnet inclusion E (~40 µm; Fig. 3e) has comparable growth relationships to garnet C, being elongated and aligned with the diamond growth zones around it, however, local diamond growth layers that may have nucleated around the inclusion cause local disruption in the regular diamond growth. The two small (<15 µm) anhedral garnet inclusions in Fig. 3f are associated with diagonal diamond growth zones that appear to be cut by the inclusions without being disrupted. Elongated subhedral garnet inclusion G (Fig. 3g ~100 µm) with both triangular and somewhat rounded terminations. The best developed crystal face (uppermost in the figure) is aligned with the local diamond growth. The inclusion is in a zone of poorly developed and irregular diamond growth layering. At >50 µm from the inclusion, diamond growth is regular and continuous growth zones enclose the inclusion.

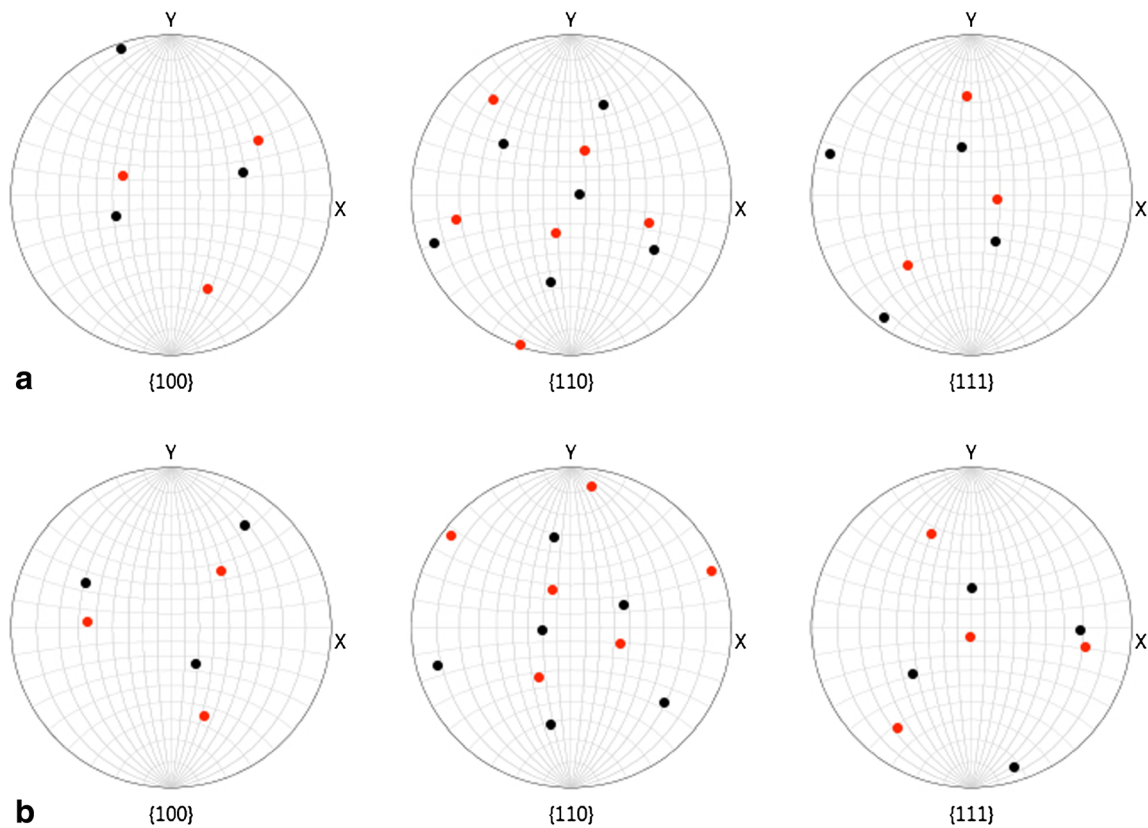


Fig. 2 a EBSD measurements of garnet inclusion JW012B (red dots) presented in pole figures showing a lower hemisphere stereographic projection onto the major crystallographic axes of the

host diamond (black dots). **b** Pole figures for garnet JW012C. Pole figures demonstrate that there is no common crystallographic orientation between the host diamond and garnet inclusions

Inclusions C to G were all exposed in a $250 \times 250 \mu\text{m}$ region of the outer core to the bottom right of the inner core. Clinopyroxene inclusion H occurs in the same region and appears to have nucleated on the inner core diamond surface and been constrained in terms of growth by this surface (Fig. 3h). The straight contact between the diamond and the omphacite is interrupted to the bottom right where another phase that is too small for analysis appears to have also nucleated on the inner core surface. Complex diamond growth can be seen to the bottom, bottom right and left of the inclusion. The inclusion-diamond contact was sampled on the left by focussed ion beam milling and the foil subsequently analysed using transmission electron microscopy (TEM). High-resolution TEM image of the contact are reported in Fig. S9 and emphasise the planar nature of the contact despite some apparent slight curvature and irregularity in the CL image (Fig. 3h). The sharp interface (Fig. S9) establishes the absence of a silica-rich fluid at the diamond-inclusion interface. In addition, scanning TEM energy dispersive X-ray fluorescence (EDX) elemental mapping established that there are no significant elemental impurities, other than nitrogen, in the diamond.

There are no coincidences in crystallographic orientation between diamond JW204 and its inclusions (Fig. S4). Four garnet inclusions that occur within $200 \mu\text{m}$ (E, 2 times F and

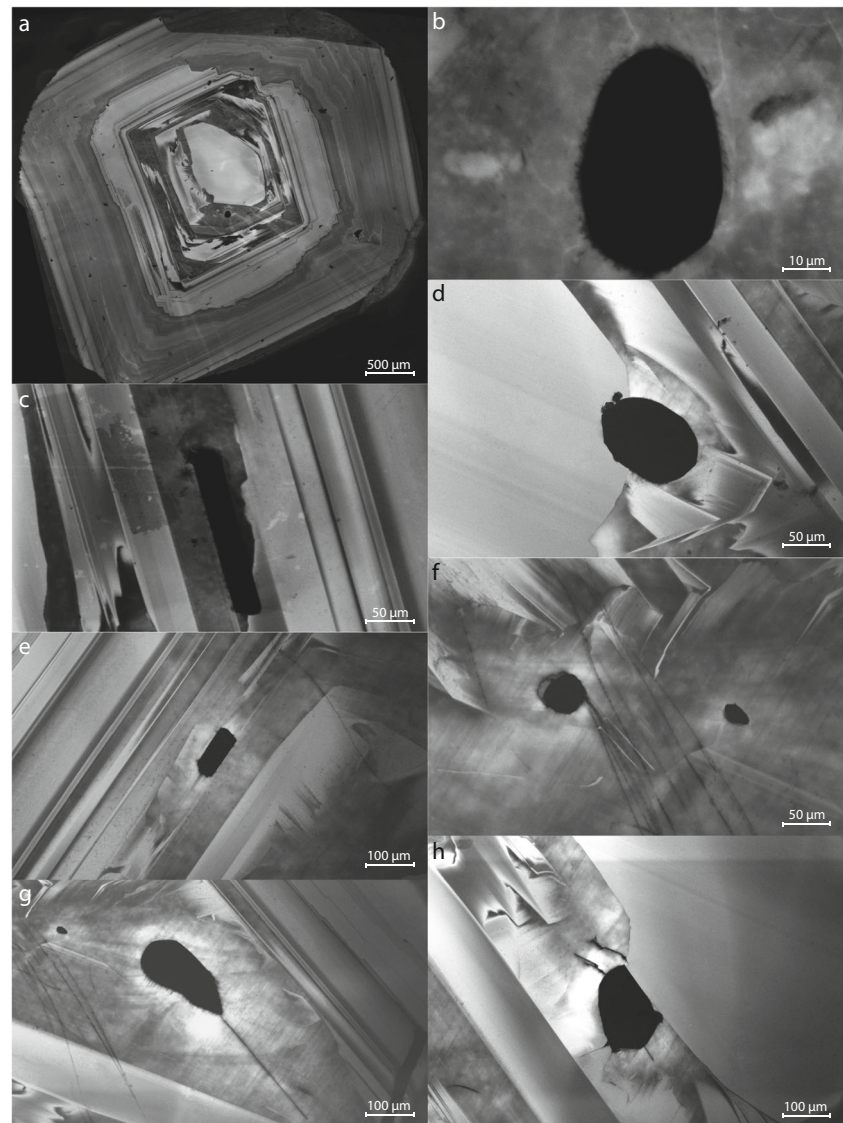
G) have crystallographic orientations within 15° deviation of the principal diamond axes, perhaps suggesting a common nucleation mechanism that is distinct from the adjacent inclusion D (located within $150 \mu\text{m}$).

Diamond JW288 contains garnet, omphacite and sulphide inclusions and is characterized by well-defined octahedral growth pattern throughout (Fig. S5a). A garnet inclusion was exposed in the low luminescent centre of the diamond (Fig. S5b) and although damaged during polishing, it appears to have faces aligned subparallel to diamond growth. The crystallographic orientation of the inclusion is distinct with respect to the orientation of the host diamond (Fig. S5c).

Dodecahedron JW334 is garnet- and omphacite-bearing (Fig. S6a). An asymmetric hexagonal core comprises several irregular areas with variable nitrogen content. The majority of the plate records irregular octahedral growth layers with some resorption planes. The rim has irregular form but octahedral growth with lower nitrogen content and little resorption of stepped faces. An ovoid anhedral garnet inclusion exposed in the inner core (Fig. S6b). The inclusion is in a region of poorly defined diamond growth but enclosed by regular growth zones at a distance of $\sim 100 \mu\text{m}$. The pole figures show no coincidences between diamond and garnet (Fig. S6c).

Diamond JW338 is a garnet-bearing octahedron (Fig. 4a) with octahedral growth habit throughout with the brightest CL

Fig. 3 **a** Composite CL image of a central plate through garnet-, omphacite- and sulphide-bearing octahedral diamond JW204. The core of the sample shows octahedral growth. Inclusions B and C are exposed in the outer core below and to the right of the core. **b** Garnet B has both rounded and well-developed crystal faces. **c** Garnet C is elongated parallel to local diamond growth. **d** Garnet D cuts the well-developed resorption surface around the inner core. **e** Euhedral garnet E is elongated parallel to diamond growth layering. **f** Two subhedral garnets occur in an area with weakly developed diamond growth layering but cut the growth. Dark linear features near the inclusions are minor cracks generated by pressure release during polishing. **g** Elongated garnet G has rounded and triangular terminations with the best developed face parallel to diamond growth. **h** Omphacite H occurs on the well-developed resorption surface around the inner core with complex diamond growth layers that nucleated from the diamond and inclusion surfaces. See text for more detailed discussion. Pole figures presented in Fig. S3



in the core. Minor hummocky cuboid growth is present at the apices of the inner rim. A garnet inclusion ($\sim 60 \mu\text{m}$; Fig. 4b) occurs at an irregular surface in the inner core. The inclusion is elongated parallel to diamond growth and does not cut growth zones and is enclosed by diamond lacking clear growth zonation that is dark in CL. A second garnet inclusion ($\sim 125 \mu\text{m}$; Fig. 4c) occurs in a region of well-defined diamond growth layering and is elongated parallel to the growth. Diamond growth zonation immediately around the inclusion is poorly defined but the inclusion is surrounded within $\sim 50 \mu\text{m}$ by well-defined growth zones. The pole figures show no coincidences between diamond and the garnets (Figs. S7a,b).

Dodecahedron JW356 is garnet-omphacite-rutile-sulphide-bearing (Fig. 5a). The core has highly complex growth with apparent resorption surfaces and variable N contents. More regular octahedral growth occurs in the rim. A subhedral ovoid garnet ($70 \mu\text{m}$) occurs in the innermost core (Fig. 5b). The inclusion has both rounded and well-developed faces.

Diamond growth immediately around the inclusion is homogeneous and growth layering is only developed at a distance of $\sim 60 \mu\text{m}$. A second anhedral garnet ($\sim 40 \mu\text{m}$) (Fig. 5c) occurs in the mid core and has both rounded and well-developed faces and is surrounded by an irregular growth zone. CL growth layers around it are partly disrupted by decompression cracks produced during polishing. The growth layers generally follow the morphology of the inclusion but have irregular contacts with surrounding diamond growth.

Four inclusions were exposed in the core by subsequent polishing. A rutile inclusion ($\sim 140 \mu\text{m}$; Fig. 5d) is positioned in relatively dark CL within the outer core. The inclusion has a rounded termination at its thickest end (top) but well developed cubo-octahedral faces at the bottom (Fig. 5d). Again diamond growth layering immediately around the inclusion is poorly defined but the inclusion is surrounded within $\sim 20 \mu\text{m}$ by concentric well-defined hummocky/cuboid growth layers. A local dark CL halo obscures the diamond

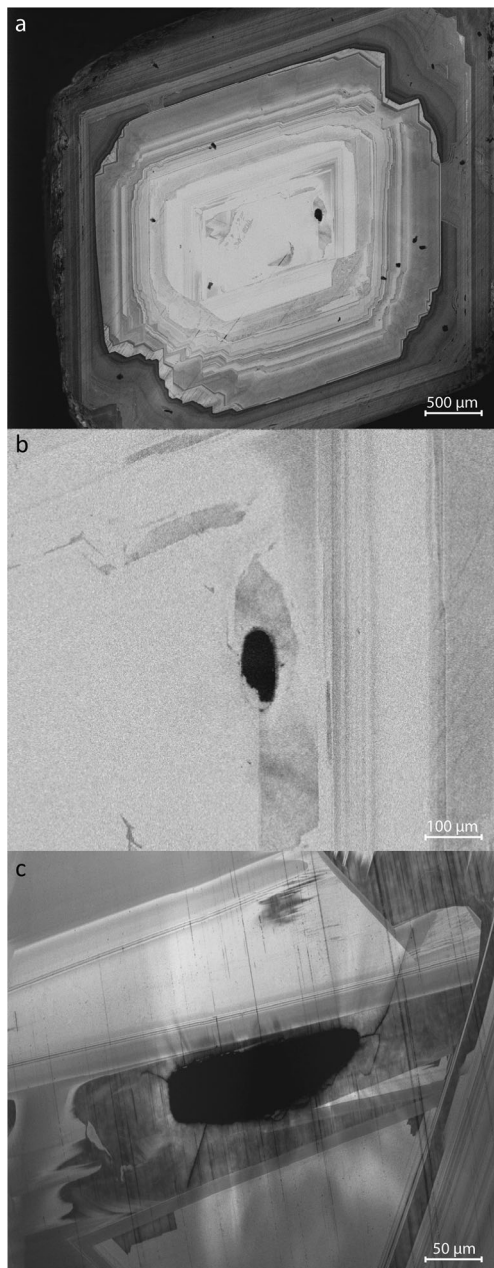


Fig. 4 **a** Composite CL image of a central plate through octahedral garnet-bearing diamond JW338 that records octahedral growth habit throughout. **b** The elongated and irregular garnet inclusion B occurs to the right of the centre on a resorption surface. **c** Elongated garnet inclusion in the outer core. Pole figures show no coincidences between diamond and inclusions (Fig. S6)

growth zones. The elongated subhedral garnet inclusion (~50 μm; Fig. 5e) has rounded and straight crystal faces and is surrounded by complex and cross cutting diamond growth. The euhedral omphacite inclusion F (~75 μm; Fig. 5f) has well-developed cubo-octahedral faces and occurs in a zone of poorly defined growth layering with dark CL but cuts a dark growth zone and is surrounded by diamond growth in at least 3 different directions. A second omphacite inclusion (~55 μm; Fig. 5g) has an elongated ovoid subhedral shape

with both rounded and well-developed faces. Although diamond growth immediately around the inclusion is poorly defined, it encloses the inclusion and has cross-cutting relationships with larger scale regular diamond growth and is enclosed by a zone of poorly defined growth layers with dark CL.

None of the inclusions in JW 356 have crystallographic orientations coincident with the host diamond (Fig. S8). Garnet inclusions B and C are 450 μm apart and in different growth zones within the core and have indistinguishable chemical compositions (Table S1). The long axes of the inclusions have different orientation (~NW-SE and E-W) and the different inclusions record crystallographic orientations that differ by 10°.

Discussion

Origin of inclusions in diamonds

Different minerals (cubic chromite and garnet, hexagonal monosulphide, monoclinic pyroxene and orthorhombic olivine) included in diamond commonly reveal cubo-octahedral morphologies that appear to have been imposed by their cubic diamond hosts (e.g., Meyer 1987). The observation of apparent epitaxy between inclusions and diamond host has been used as evidence that diamond and inclusion growth are contemporaneous and hence strong proof of syngeneses (Futergendler and Frank-Kamenetsky 1961; Orlov 1977; Sobolev 1977; Harris and Gurney 1979; Meyer 1987; Bulanova 1995). These previous observational and X-ray studies focussed mainly on peridotitic inclusion assemblages including a study of diamond growth around peridotitic chromite that reported a syngenetic relationship based on the 3D growth and EBSD relationships (Wiggers de Vries et al. 2011). Expanding on previous studies (e.g., Harris and Gurney 1979), the data reported here represent the first integrated study of inclusion morphology, inclusion and diamond crystallographic orientation and diamond growth form from inclusions-bearing diamonds of eclogitic paragenesis.

Crystallographic orientation

All 24 individual inclusions and the eight host diamonds have homogeneous crystallographic orientations demonstrating all are monocrystalline despite multiple growth and resorption zones (Figs. 1a-5a), implying epitaxial diamond growth. Crystallographic coincidence between the host diamond and an inclusion would indicate control of the diamond on the mineral inclusion orientation, implying syngenetic growth (e.g., Harris and Gurney 1979). The pole figures (Figs. 2; S2-8) establish that none of the inclusions have alignment of their major crystal axes with the host diamond ruling out

Fig. 5 **a** Composite CL image of a central plate through octahedral garnet- omphacite- sulphide- and rutile-bearing diamond JW356. **b** Garnet B has both rounded and well-developed faces. **c** Garnet C occurs in the mid core with both rounded and well-developed faces. The second polish exposed four further inclusions. **d** Rutile inclusion D. **e** Elongated garnet inclusion E. The light band to the upper right of the inclusion is a milling artefact. **f** Omphacite F has cubo-octahedral faces and occurs in a zone of poorly defined growth layering. **g** Omphacite G has both rounded and well-developed faces. Pole figures are presented in Fig. S6



epitaxy. Garnet inclusion JW078C records a mirror pattern with respect to diamond crystal axes on the pole figures (Figs. S2e), although there is no alignment of the major crystal axes. The mirror pattern and one indistinguishable Euler angle (Table S3) implies that host and inclusion share one common, relatively low index crystal plane, however the mis-alignment of major crystal axes shows there is no well-defined orientation relationship. Therefore, in contrast to some previous studies that have found unambiguous evidence of inclusion-diamond epitaxy (e.g., Wiggers de Vries et al. 2011), this work finds no examples, although garnet JW078c implies that diamond had some crystallographic control on garnet growth.

Multiple inclusions have been characterised in two diamonds (JW204 = 8 and JW356 = 7). Four associated garnets in plate JW204 (E, F1, F2, G) occur in a 300 times 250 µm area of the outer core and have indistinguishable mineral compositions (Table S1) and crystallographic orientations that are within 5–15° of each other (Fig. S4). Euler angles (Table S3) show the garnets are orientated within 2 and 6° of each other.

Two garnets in JW356 occur 400 µm apart but in different growth zones (inner core and outer core; B and C). Again, mineral compositions are indistinguishable and crystallographic orientations are within ~5° (Fig. S1), as are Euler angles (Table S3). The two omphacites from the same sample (F and G) have comparable mineral compositions and some crystallographic orientations within ~10° but Euler angles differ by up to 30° (Table S3).

Based on multiple olivine inclusions in diamond with the same orientation as diamond, Nestola et al. (2014) and Milani et al. (2016) proposed that such olivines could have a protogenetic origin formed by selective partial dissolution of a single originally larger grain. Although the crystallographic orientations of the three groups of inclusions studied here are generally within 2–15°, the angular differences in orientation are significantly larger than analytical error. Moreover, other inclusions occur in the same regions that have markedly different crystallographic orientation (e.g., JW204C). Further evidence against a single parent grain acting as a protogenetic

source in these cases is given by the inclusion morphology. Garnet inclusions JW204E and JW204G have well developed crystal faces related to local diamond growth, as does JW356F. We therefore favour a model whereby inclusion morphology and crystallographic orientation is generally influenced by diamond growth. Once nucleated on a diamond surface, inclusion morphology is controlled by diamond growth. Adhesion energies between diamond and silicates are, however, too low to force epitaxial growth of inclusions and diamond (Bruno et al. 2016).

Further evidence for diamond having crystallographic control on the lattice orientation of at least a proportion of inclusions is provided by previous work. Wiggers de Vries et al. (2011) reported that all crystallographic planes in a magnesiochromite inclusion and host diamond were sub-parallel with coincident lattice planes. Milani et al. (2016) demonstrate the absence of epitaxial relationships between olivine and host diamond, importantly, however, there is a tendency for the olivine [010] axes to plot on the great circles linking the major crystal axes of diamond. This implies that the inclusion-diamond orientation relationships may not be random. Together these data suggest a crystallographic control was operating during the formation of these inclusion–host pairs and supports a syngenetic origin.

Inclusion morphology and diamond growth features

Based on the discussion above, we argue that inclusion morphology and inclusion-diamond growth relationships appear key to assessing the genesis of inclusions. Here our interpretation contrasts with recent publications by Nestola and co-workers (Nestola et al. 2014, 2017; Agrosi et al. 2016; Nimis et al. 2016) who argue that protogenetic phases could take on cubo-octahedral form during or after entrapment in diamond. Under conditions of diffusion creep, there would have to be diffusion of carbon and the elements in the silicate inclusions from interfaces with high normal stress, to the interfaces with low normal stress. The extremely low observed and inferred self-diffusivity of carbon and nitrogen in diamond (e.g., Harte et al. 2009; Craven et al. 2009; Zhang and Wu 2012) implies that diffusion creep is not a viable mechanism to cause cubo-octahedral morphology on inclusions post entrapment. Moreover, creep-controlled processes would be expected to cause internal deformation, which has not been observed (Nestola et al. 2014; Agrosi et al. 2016). Nimis et al. (2016) reported silicate inclusions were surrounded by a thin film of hydrous silicic fluid ($< 1.5 \mu\text{m}$). Post entrapment development of euhedral crystal faces on silicate inclusions due to new growth from such a fluid film is considered unfeasible due to its small volume and the fact that multiple types of silicates have been reported with imposed cubo-octahedral morphology.

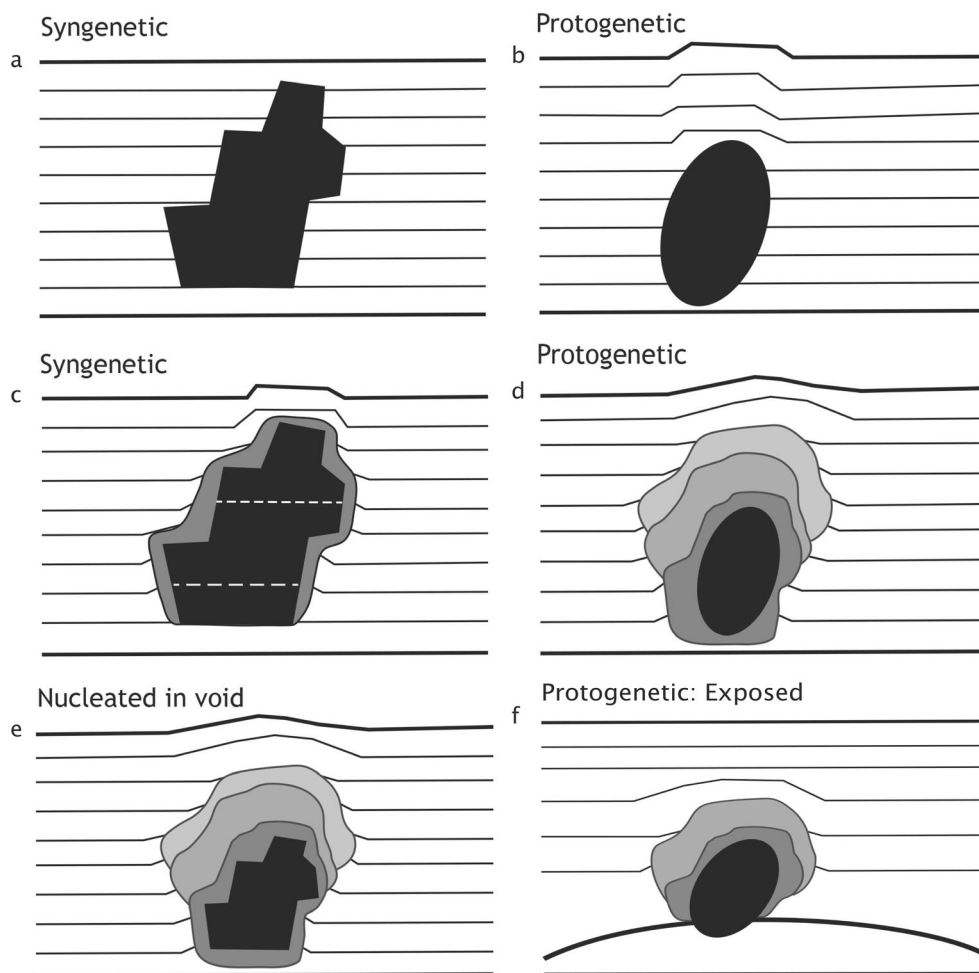
We argue that disturbances, or the lack thereof, in regular diamond growth patterns are important parameters for determining the genesis of an inclusion, based on the CL images. Bulanova (1995) proposed a model whereby disturbed growth around an inclusion is a strong indicator for protogenesis whereas syngenetic inclusions cut off growth zones and do not disturb new diamond growth (Fig. 6). This model implies diamond growth in the vicinity of an inclusion occurs on one interfacial surface. The model does not specifically take into account potential different growth rates of diamond and the inclusion. To continue to grow, the inclusion must have access to the metasomatic agent but if inclusion growth stops, its surfaces could potentially act as a surface for diamond nucleation. The small size of the inclusions with respect to their host diamonds implies inclusion growth would not significantly change the composition of the metasomatic medium. Hence mineral compositions are not expected to change significantly during growth. Subsequent diffusion during storage in the mantle would, however, tend to homogenise any compositional zonation.

A second scenario not fully covered by the Bulanova model is when a mineral nucleates and forms within the metasomatic agent. The inclusion would again provide surfaces for potential diamond nucleation and growth. Distinguishing diamond growth relationships in such a situation from those around a protogenetic inclusion would be difficult (see Fig. 6).

Although the CL images do not provide full 3D growth patterns, there is sufficient evidence to establish that diamond growth immediately around many inclusions is often poorly defined (e.g., Figs. 1a, b, S3 a,b) and possibly partly obscured by bright and dark CL halos. A previous study by Wiggers de Vries et al. (2011) suggested that a CL halo around a chromite grain was caused by elemental impurities in the diamond. The TEM analysis of omphacite inclusion JW204H establishes that this is not the case. These data establish that the CL halo is not due to compositional difference and hence maybe charging artefacts but that the poorly defined diamond growth, often mottled in appearance, is an original feature.

Growth relationships of two inclusions in sample JW204 appear to provide unambiguous evidence of contrasting modes of origin. Garnet JW204D (Fig. 3d) cuts a major resorption surface between the inner and outer core of the diamond. Crystal faces within the inner core are well-developed and contrast with more rounded resorption faces in the outer core. Diamond growth around the inclusion and at the resorption surface of the outer core is complex and contrasts with the regular growth that occurs further from the resorption surface, $> 50 \mu\text{m}$ (Fig. 3d). These observations establish that the core of the diamond was resorbed, exposing the inclusion to resorption resulting in the partially rounded morphology. Subsequent diamond nucleated on the surface of the core and the inclusion, resulting in the observed complex diamond growth. The inclusion is protogenetic to the outer core, but the

Fig. 6 Schematic representations of the interaction of inclusions with diamond during diamond growth around protogenetic and syngenetic inclusions. **a** and **b** show the interaction between syngenetic and protogenetic inclusions, as proposed by Bulanova (1995). **c** and **d** include the nucleation of diamond around the inclusions (grey area). **e** includes the multistage nucleation of diamond around a syngenetic inclusion nucleated from the diamond forming agent. **f** includes the nucleation of diamond around a protogenetic inclusion exposed following a diamond resorption event. Dark growth lines indicate major diamond growth/resorption boundaries



well-developed crystal faces of the inclusion in the inner core suggest a probable syngenetic relationship with the diamond core.

Omphacite JW204H in contrast has nucleated on the inner core resorption surface (Fig. 3h). Diamond growth from the resorption surface and around the inclusion is not well defined but involves multiple nucleation points and different growth directions (see also Fig. S9a) before regular, larger scale growth zones were established $\sim 100 \mu\text{m}$ from the resorption surface. This inclusion appears syngenetic to the outer core but the observed complex growth does not readily conform to the growth model of Bulanova (1995). In fact, the majority of the studied inclusions have complex relationships with the host diamond. This point is emphasised in Table 1 where inclusion growth forms and their relationships with the host diamond are summarised. Perhaps the most important observation is that 17 of the 24 inclusions are immediately surrounded by diamond with irregular or undefined growth zonation indicating rapid diamond growth. In addition, the majority of these inclusions (12 of 17) are enclosed on the larger scale (50–100 μm) by regular diamond growth zones (e.g., Figs. 1, 3, 4 and 5). These relationships are possibly best

observed around inclusion JW356G (Fig. 5g) and are interpreted as evidence of rapid diamond nucleation and irregular growth around an inclusion followed by the establishment of more regular diamond growth zonation controlled by the overall shape of the diamond. As shown schematically in Fig. 6, these relationships cannot be used to establish if the inclusions formed syngenetically by nucleation within the diamond forming agent or if an existing mineral was entrapped in the agent. If the inclusion acts as a nucleation surface for diamond growth, the two modes of origin would produce similar diamond growth around the inclusion. Under such scenarios, it is only possible to distinguish between a syngenetic and protogenetic origin if the morphology of the inclusion is diagnostic.

Consideration of inclusion morphology, crystallographic orientation and relationship to host diamond growth is needed to constrain inclusion origin. Table 2 summarises the key findings used to propose if inclusions are considered syngenetic or protogenetic. The crystallographic relationship between garnet JW078C and the host diamond presents unambiguous evidence that garnet JW078C crystallised synchronously and we argue that there is no viable process that

Table 2 Summary of diagnostic morphological and crystallographic features

Sample No.	Unknown Origin	Protogenetic Cuts resorption surface	Syngenetic				Enclosed growth & euhedral faces
			Epitaxy	Cubo-Octa growth	Nucleation on growth surface	Aligned with diamond growth	
JW012							B,C
JW078			C	B,C			
JW145							C
JW204	B,F	D		B,D	H	C,E	G
JW288						B	
JW334	B						
JW338					B	B, C	C
JW356	B			D,F			C,D,E,G

can explain formation of inclusions with imposed cubo-octahedral faces other than crystallisation in the presence of a diamond forming fluid or melt; i.e., synchronous crystallisation (JW078B,C; JW204B,D; JW356D, F; cf. Nestola et al. 2014, 2017).

Inclusions with well-formed crystal faces nucleated on diamond growth surfaces (JW204H; JW338B) or subhedral/euhedral inclusions aligned with diamond growth also represent syngenetic growth (JW204C,E,F; JW288B; JW338B,C). Inclusion growth may lead to disruption of diamond growth on the local scale (< 50 µm; JW204E, G, H; JW338C; JW356C,D,E,G) but at a larger scale (>50 µm) the orientation of the inclusion is controlled by diamond growth. Seventy percent of the studied inclusions are in diamond with localised poorly developed growth zonation but are surrounded by well-defined growth within 100 µm (Tables 1 and 2). Several of these “enclosed” inclusions have well-developed crystal faces aligned with diamond growth (e.g., JW012C; JW204G) indicating syngeneity even when imposed cubo-octahedral faces are not fully developed.

Inclusions JW204F1 and JW204F2 are anhedral and cut diamond growth zonation without causing any disruption. Based on the Bulanova (1995) model these inclusions would be interpreted as syngenetic but we consider the morphological relationships not to be sufficiently well developed to rule out a protogenetic origin.

Of the 24 studied inclusions, we conclude that 19 record morphology and/or orientation that implies syngenetic formation with the host diamonds. Garnet 204D records both proto- and syngenetic relationships. The well-developed crystal faces in the inner core are taken as evidence of syngenetic formation with the inner core. The inclusion cuts the resorption interface between the inner and outer core, clearly establishing that the grain is protogenetic with respect to the outer core.

Nestola et al. (2017) proposed the term synchronous to describe protogenetic inclusions that had undergone re-equilibration with the diamond forming agent. Temperatures in the mantle lithosphere are sufficiently high that diffusive

exchange between a protogenetic inclusion and the volatile-rich diamond forming agent is essentially instantaneous on a geological timescale (e.g., see discussion in Koornneef et al. 2017). Hence chemically protogenetic inclusions would be generally expected to record the mantle environment at the time of their entrapment. Hence, we do not favour the use of the term synchronous to describe mineral inclusions with clear evidence of well-formed crystal faces as this relationship implies syngenetic crystallisation of the inclusion and host diamond. However, based on inclusion JW204D that occurs in two distinct diamond growth zones, the synchronous concept proposed by Nestola et al. (2017) is valuable. Inclusion JW204D originally formed in the inner core of the diamond but compositional data would record the time of last equilibration with a diamond forming agent, i.e., the time of outer core formation.

Conclusions

Eclogitic mineral inclusions in gem quality diamonds from Jwaneng, Botswana were trapped by multiple mechanisms. Despite complex growth and resorption, individual diamonds have homogeneous epitaxial growth. All individual inclusions have homogeneous crystallographic orientation and no resolvable compositional zonation. Nineteen inclusions show some well-developed crystal faces and six (partial) imposed cubo-octahedral morphology. Six inclusions have crystal faces orientated parallel to diamond growth zones and/or appear to have nucleated on a diamond growth surface, implying syngeneity. No inclusions record epitaxy with the host diamond. One garnet inclusion (JW 078C) records a lattice orientation implying diamond influenced its growth. These data suggest that epitaxial diamond-inclusion growth is rare and that the imposition of cubo-octahedral faces on inclusions rarely result in epitaxy. This observation is consistent with the finding that there is no difference in adhesion energies between diamond and olivine interfaces (Bruno et al. 2016)

and that by inference during synchronous growth there is no reason for silicate minerals to develop preferential crystallographic orientations.

In most cases, diamond growth layers immediately around inclusions (<20 µm) are poorly defined and in some cases nucleated from the inclusion. At the larger scale, 50–100 µm, most inclusions are enclosed by well-defined diamond growth layering. Four inclusions influence surrounding diamond growth. These observations could indicate a syn- or proto-genetic origin. Inclusion clusters that occur in different growth zones have indistinguishable compositions and in some cases crystallographic orientations within 5 and 15°. The different orientations argues against formation from an original single mineral grain and suggests that diamond growth influenced inclusion growth. We therefore favour a model whereby inclusion morphology and alignment are generally influenced by diamond growth but this relationship does not necessarily produce epitaxy.

Individual diamonds contain inclusions that record evidence of both syngenetic and protogenetic relationships with the host. One inclusion is syngenetic to the diamond core but protogenetic to the growth zone that surrounds 70% of the inclusion. In this context the term synchronous growth (Nestola et al. 2017) is useful because at mantle temperatures relatively rapid elemental diffusion would mean the inclusion retained geochemical and age information related to formation of the outer core.

Acknowledgements Debswana Diamond Company and The De Beers Group of Companies are thanked for allowing access to run of mine production and diamond donation. Gassan Diamonds and particularly Pieter Ouwerkerk are thanked for help with diamond polishing. Constructive reviews and comments by Jeff Harris and Fabrizio Nestola and guest editor Thomas Stachel are gratefully acknowledged. Travel for sampling was sponsored by Stichting dr Schürmannfonds.

Open Access This article is distributed under the terms of the Creative Commons Attribution 4.0 International License (<http://creativecommons.org/licenses/by/4.0/>), which permits unrestricted use, distribution, and reproduction in any medium, provided you give appropriate credit to the original author(s) and the source, provide a link to the Creative Commons license, and indicate if changes were made.

References

- Agrosi G, Nestola F, Tempesta G, Bruno M, Scandale E, Harris J (2016) X-ray topographic study of a diamond from Udachnaya: implications for the genetic nature of inclusions. *Lithos* 248:15–159
- Bruno M, Rubbo M, Aquilano D, Massaro F, Nestola F (2016) Diamond and its olivine inclusions: a strange relation revealed by ab initio simulations. *Earth Planet Sc Lett* 435:31–35
- Bulanova G (1995) The formation of diamond. *J Geochem Explor* 53:1–23
- Bunge H (1993) Texture analysis in materials science: mathematical methods. Cuvillier Göttingen, 593 pp
- Chantler CT, Olsen K, Dragoset RA, Chang J, Kishore AR, Kotochigova SA, Zucker DS (2005) X-Ray Form Factor, Attenuation and Scattering Tables (version 2.1). [Online] Available: <https://www.physics.nist.gov/ffast>
- Craven JA, Harte B, Fisher D, Schulze DJ (2009) Diffusion in diamond. I. Carbon isotope mapping of natural diamond. *Mineral Mag* 73:193–200
- Futergendler S, Frank-Kamenetsky V (1961) Oriented inclusions of olivine, garnet and chrome-spinel in diamonds. *Zapisky Vsesoyuznogo Mineralogicheskogo Obshchestva* 90:230–236
- Gress MU, Howell D, Chinn IL, Speich L, Kohn SC, van den Heuvel Q, Schulten E, Pals ASA, Davies GR (2018) Episodic diamond growth in the Kaapvaal Craton beneath Jwaneng mine, Botswana. *Miner petrol*, this volume
- Harris J, Gurney J (1979) Inclusions in diamond. *The Properties of Diamond*: 555–591
- Harte B, Taniguchi T, Chakraborty S (2009) Diffusion in diamond. II. High-pressure–temperature experiments. *Mineral Mag* 73:201–204
- Koomneef JM, Gress MU, Chinn IL, Jelsma HA, Harris JW, Davies GR (2017) Archaean and Proterozoic diamond growth from contrasting styles of large-scale magmatism. *Nat Commun* 8:648
- Meyer HOA (1987) Inclusions in diamond. In: Nixon PH (ed) *Mantle xenoliths*. John Wiley and Sons Chichester, pp 501–522
- Milani S, Nestola F, Angel RJ, Nimis P, Milani S, Bruno M, Prencipe M, Harris JW (2016) Crystallographic orientations of olivine inclusions in diamonds. *Lithos* 265:312–316
- Nestola F, Nimis P, Angel R, Milani S, Bruno M, Prencipe M, Harris J (2014) Olivine with diamond-imposed morphology included in diamonds. Syngensis or protogenesis? *Int Geol Rev* 56:1658–1667
- Nestola F, Jung H, Taylor LA (2017) Mineral inclusions in diamonds may be synchronous but not syngenetic. *Nat Commun* 8:14168
- Neuser R, Schertl H-P, Logvinova A, Sobolev N (2015) An EBSD study of olivine inclusions in Siberian diamonds: evidence for syngenetic growth? *Russian Geol Geophys* 56:321–329
- Nimis P, Alvaro M, Nestola F, Angel R, Marquardt K, Rustioni G, Harris J, Marone F (2016) First evidence of hydrous silicic fluid films around solid inclusions in gem-quality diamonds. *Lithos* 260:384–389
- Orlov YL (1977) *The mineralogy of the diamond*. John Wiley and Sons, 235 pp
- Prior D, Boyle A, Brenker F et al (1999) The application of electron backscatter diffraction and orientation contrast imaging in the SEM to textural problems in rocks. *Am Mineral* 84:1741–1759
- Shirey SB, Cartigny P, Frost DJ, Keshav S, Nestola F, Nimis P, Pearson DG, Sobolev NV, Walter MJ (2013) Diamonds and the geology of mantle carbon. In: Hazen RM, Jones AP, Baross JA (eds) *Carbon in Earth*. *Rev Mineral Geochem*, vol 75. Mineral Soc Am, Chantilly, pp 355–421
- Sobolev N (1977) Deep-seated inclusions in kimberlites and the problem of the compositions of the upper mantle. *American Geophysical Union*, Washington, DC. Translated by DA Brown from Russian edition (1974). Novosibirsk, Russia, Nauka (in Russian)
- Timmerman S, Matveev S, Gress M, Davies G (2015) A methodology for wavelength dispersive electron probe microanalysis of unpolished silicate minerals. *J Geochem Explor* 159:243–251
- Timmerman S, Chinn IL, Fischer D, Davies GR (2018) Formation of unusual yellow Orapa diamonds. *Miner petrol*, this volume
- Wiggers De Vries D, Drury M, De Winter D, Bulanova G, Pearson D, Davies G (2011) Three-dimensional cathodoluminescence imaging and electron backscatter diffraction: tools for studying the genetic nature of diamond inclusions. *Contrib Mineral Petrol* 161:565–579
- Zhang B, Wu X (2012) Calculation of self-diffusion coefficients in diamond. *Appl Phys Lett* 100:051901